INFECTION AND IMMUNITY, Apr. 2008, p. 1340–1348 Vol. 76, No. 4
0019-9567/08/$08.00+0 doi:10.1128/IAI.00778-07

Lactobacillus rhamnosus Strain GG Prevents Enterohemorrhagic *Escherichia coli* O157:H7-Induced Changes in Epithelial Barrier Function▽

K. C. Johnson-Henry,[1]† K. A. Donato,[1,2]† G. Shen-Tu,[1] M. Gordanpour,[1] and P. M. Sherman[1,2]*

Research Institute, Hospital for Sick Children,[1] and Departments of Paediatrics and Laboratory Medicine & Pathobiology,[2] University of Toronto, Toronto, Ontario, Canada

Received 8 June 2007/Returned for modification 15 August 2007/Accepted 22 January 2008

Enterohemorrhagic *Escherichia coli* (EHEC) O157:H7 intimately attaches to intestinal epithelial monolayers and produces attaching and effacing (A/E) lesions. In addition, EHEC infection causes disruptions of intercellular tight junctions, leading to clinical sequelae that include acute diarrhea, hemorrhagic colitis, and the hemolytic-uremic syndrome. Current therapy remains supportive since antibiotic therapy increases the risk of systemic complications. This study focused on the potential therapeutic effect of an alternative form of therapy, probiotic *Lactobacillus rhamnosus* strain GG, to attenuate EHEC-induced changes in paracellular permeability in polarized MDCK-I and T84 epithelial cell monolayers. Changes in epithelial cell morphology, electrical resistance, dextran permeability, and distribution and expression of claudin-1 and ZO-1 were assessed using phase-contrast, immunofluorescence, and transmission electron microscopy and macromolecular flux. This study demonstrated that pretreatment of polarized MDCK-I and T84 cells with the probiotic *L. rhamnosus* GG reduced morphological changes and diminished the number of A/E lesions induced in response to EHEC O157:H7 infection. With probiotic pretreatment there was corresponding attenuation of the EHEC-induced drop in electrical resistance and the increase in barrier permeability assays. In addition, *L. rhamnosus* GG protected epithelial monolayers against EHEC-induced redistribution of the claudin-1 and ZO-1 tight junction proteins. In contrast to the effects seen with the live probiotic, heat-inactivated *L. rhamnosus* GG had no effect on EHEC binding and A/E lesion formation or on disruption of the barrier function. Collectively, these findings provide in vitro evidence that treatment with the probiotic *L. rhamnosus* strain GG could prove to be an effective management treatment for preventing injury of the epithelial cell barrier induced by A/E bacterial enteropathogens.

Enterohemorrhagic *Escherichia coli* (EHEC) O157:H7 infection is a common cause of intestinal disease in humans (43). Intestinal infections are known to mediate multiple changes in host cellular signal transduction responses, which impair epithelial transport and the barrier function (9). The current treatment remains predominantly supportive because antibiotics appear to increase the risk of systemic complications (e.g., the hemolytic-uremic syndrome), perhaps by releasing Shiga-like toxins from the bacterial cell periplasm into the gut lumen (43).

The intestinal tract is comprised of a mucosal epithelial cell barrier, which is critical in providing the first line of defense against external insults (24). Tight junctions represent the luminal-most portion of a broader "apical junction complex" that circumscribes polarized epithelial cells (44). Tight junction domains are comprised of integral membrane proteins, including the junction adhesion molecule, occludin, and members of the claudin superfamily, which differentially modulate the transport of ions and macromolecules and prevent toxin, antigen, and microflora interactions with subepithelial tissues (28, 44). The primary purpose of claudins is to regulate the paracellular flow of ions and small molecules mediated through extracellular loops that protrude into the spaces between adjacent cells (44). These integral proteins are connected to cytoplasmic plaque proteins, including ZO-1, which anchor tight junctions to the F-actin cytoskeleton for mechanical regulation (28). Disruption of epithelial tight junctions due to *E. coli* O157:H7 infection depends on bacterial attachment and the deployment of a type III secretion system (encoded by the locus of enterocyte effacement), which acts as a molecular syringe to transmit bacterial effector proteins into the cytoplasm of host cells (32, 45). As a result, cascades of signal transduction events cause F-actin pedestal formation (mediated by actin bridging proteins, including α-actinin), the loss of microvilli, and attaching and effacing (A/E) lesions (22).

Probiotics, including *Lactobacillus* species, are defined as live microorganisms which have beneficial effects for the host (8). Increasing evidence indicates that probiotics are effective in preventing and treating a variety of intestinal disorders, including pouchitis, traveler's diarrhea, antibiotic-associated diarrhea, and acute infectious diarrhea (33). Probiotics exert their beneficial effects by a variety of complementary mechanisms, including an ability to modulate host innate immune responses, such as secretion of mucins from goblet cells, adaptive immune responses, protection from the damaging effects of aspirin, and competitive exclusion of pathogens (36). In addition, we have previously shown that probiotics have the

* Corresponding author. Mailing address: Hospital for Sick Children, Room 8409, 555 University Avenue, Toronto, Ontario, Canada M5G 1X8. Phone: (416) 813-7734. Fax: (416) 813-6531. E-mail: philip.sherman@sickkids.ca.

† K.C.J.-H. and K.A.D. contributed equally to this research.

▽ Published ahead of print on 28 January 2008.

ability to decrease *Citrobacter rodentium*-induced mucosal inflammation and disruption of paracellular junctions (20).

Lactobacillus rhamnosus strain GG is a gram-positive, lactic acid-producing bacterium that was first isolated from the stools of a healthy human (7, 10). *L. rhamnosus* GG has been employed experimentally as a supplement to the human neonatal intestinal microflora and has been studied to determine its effects on the enhancement of immunoglobulin (Ig) secretion. This probiotic prevents rotavirus-induced diarrhea, *Salmonella* infection in vitro, and the recurrence of colitis (7, 10), and it protects against indomethacin-induced changes in barrier function both in humans and in polarized intestinal cell monolayers grown in tissue culture (11). A notable characteristic of this bacterium is its ability to adhere to epithelial cells in tissue culture and displace intestinal pathogens, including *E. coli* (23).

The maintenance of the cytoskeleton and tight junction integrity of polarized epithelial monolayers plays an integral role in modulating paracellular diffusion. This epithelial barrier function can be weakened by infection with bacteria, including pathogenic *E. coli* strains (39). Therefore, the aim of this study was to determine the potential ability of *L. rhamnosus* GG to protect the epithelial cell barrier in response to challenge with the enteric pathogen *E. coli* O157:H7 and to delineate the mechanistic aspects by which *L. rhamnosus* GG exerts its effects.

[Part of this research was presented at the 6th International Symposium on Shiga Toxin (Verocytotoxin)-Producing *Escherichia coli* Infections (VTEC 2006), Melbourne, Australia.]

MATERIALS AND METHODS

Bacterial strains, cell cultures, and growth conditions. *L. rhamnosus* strain GG (ATCC 53103) was purchased frozen from the American Type Culture Collection (Manassas, VA), was cultured on blood agar (Difco, Detroit, MI), and was grown in de Mann-Rogosa-Sharpe (MRS) broth (Difco) aerobically at 37°C for 24 h. *E. coli* O157:H7 strain CL56 was grown overnight at 37°C in static, nonaerated Penassay broth (Difco, Detroit, MI).

As previously described, Madin-Darby canine kidney (MDCK-I) and T84 epithelial cells were used as model epithelia to study the dynamics of barrier function due to their ability to form polarized monolayers with high resistance (47). MDCK-I epithelial cells were kindly provided by Roger Worrell (The Vontz Center for Molecular Studies, University of Cincinnati, Cincinnati, OH), and were cultured until they were confluent in Dulbecco's modified Eagle medium (DMEM) supplemented with 10% fetal bovine serum (Invitrogen) and 2% penicillin-streptomycin (Invitrogen), as previously described (47). T84 epithelial cells were purchased from the American Type Culture Collection and grown in tissue culture flasks using established methods (37). Briefly, T84 cells were cultured using DMEM and Ham's F-12 medium (Invitrogen Canada Inc., Burlington, Canada) at a 1:1 ratio supplemented with 10% fetal bovine serum (Invitrogen), 0.6% glutamine, 1.9% sodium bicarbonate, and 2% penicillin-streptomycin (Invitrogen) until they were confluent. The cell culture medium was changed to fresh medium without antibiotics prior to treatment of the cells with bacteria.

Cells were grown in 25-cm^2 flasks (Corning, Corning, NY) until they were confluent or in Lab-Tek chamber slides (VWR International Ltd., Mississauga, Canada). In addition, T84 and MDCK-I polarized monolayers were grown on 6.5- or 12-mm-diameter Transwells (Corning) at 37°C in the presence of 5% CO_2 until the transepithelial electrical resistance (TER), as measured with a Millicell ERS voltmeter (Millipore, Bedford, MA), was greater than 1,000 $\Omega \cdot cm^2$.

Effects of viable probiotics and their products on pathogen viability. The effects of probiotics on the viability of the pathogen were assessed using coincubation methods, as previously described (20). Briefly, *L. rhamnosus* GG (10^8 CFU/ml) was coincubated at a ratio of 1:1 (vol/vol) with *E. coli* O157:H7 (10^7 CFU/ml) in Penassay broth (10 ml) for 3 and 18 h at 37°C. Serial dilutions were prepared, and 0.1-ml aliquots of 1:100,000 dilutions were spread onto MacConkey agar plates (PML Microbiologicals, Mississauga, Ontario, Canada) and incubated overnight at 37°C. Colonies were then counted, and the results were expressed as absolute numbers of CFU.

To determine if secreted products affected pathogen viability, culture supernatants were employed. Culture supernatants were prepared as previously described (20). Briefly, supernatants resulting from 4 h of growth of *L. rhamnosus* GG in MRS broth were centrifuged at 1,600 × *g* for 5 min and filtered twice through a 0.2-μm filter (Millipore). *E. coli* O157:H7 (10^8 CFU/ml) was incubated in an equal volume of *L. rhamnosus* GG culture supernatant for 18 h at 37°C and then plated onto MacConkey agar plates. Following overnight incubation at 37°C, visible bacteria were enumerated to determine the number of viable CFU.

Transmission electron microscopy. To assess epithelial cell monolayer structures, polarized epithelial cells were prepared as previously described, with minor modifications (20). Briefly, MDCK-I cells were grown on 60-mm plates at 37°C in the presence of 5% CO_2 to confluence. Confluent polarized monolayers were either infected with EHEC O157:H7 (10^7 CFU/ml) for 4 h, treated with *L. rhamnosus* GG (10^8 CFU/ml) for 4 h, pretreated for 1 h with *L. rhamnosus* GG prior to EHEC infection (3 h), or left untreated. Epithelial cell monolayers were then washed twice with phosphate-buffered saline (PBS). Fixative (2.5% glutaraldehyde in phosphate buffer) was then added to the cells and incubated at room temperature for 15 min. Cells were then scraped from the dishes and centrifuged at 41 × *g* for 10 min. The cells were subsequently fixed in osmium tetroxide for 1 h, dehydrated in a graded acetone series (50 to 100% acetone), and then embedded in epoxy resin. Ultrathin sections (80 nm) were cut with a Reichert Ultracat E (Leica Inc., Richmond Hill, Ontario, Canada). Samples were viewed with a JEM-1230 (JOEL USA Corp., Peabody, MA) transmission electron microscope operated at 80 kV. Digital images were acquired with a charge-coupled device camera (AMT Advantage HR camera system; AMT, Massachusetts) attached to the electron microscope.

Detection of *E. coli* O157:H7 adhesion and A/E lesions by alternating phase-contrast and immunofluorescence microscopy. As described previously (15, 17), indirect immunofluorescence using a murine monoclonal antibody against the F-actin bridging protein α-actinin was employed to detect *E. coli* O157:H7-induced A/E lesions. Briefly, T84 and MDCK-I cells grown overnight on chamber slides in the presence of 5% CO_2 at 37°C were washed with sterile PBS. Cells were then either infected with *E. coli* O157:H7 (10^7 CFU/ml) (3 h), treated with viable or heat-killed (100°C for 1 h) *L. rhamnosus* GG (10^8 CFU/ml) (3 h), pretreated with viable *L. rhamnosus* GG or heat-killed *L. rhamnosus* GG for 1 h at 37°C prior to EHEC infection (3 h), or left untreated. Cells were fixed in 100% cold methanol for 10 min (Caledon Laboratories, Georgetown, Ontario, Canada), and slides were examined by alternating phase-contrast and immunofluorescence microscopy at a magnification of ×40 (Leitz Dialuz 22; Leica Canada Inc., Willowdale, Ontario, Canada). A/E lesions were quantified, and the results were expressed as the number of α-actinin foci per cell. A total of ≥100 cells were counted in each experiment.

TER and dextran permeability as measurements of changes in the barrier function of polarized epithelial cell monolayers. As previously described (18), polarized MDCK-I and T84 cells were grown on 6.5-mm (pore size, 0.4 μm) or 12-mm (pore size, 0.4 μm) Transwells (Corning) and cultured until the TER reached a minimum of 1,000 $\Omega \cdot cm^2$. Cells were infected with EHEC (10^7 CFU/ml), treated with *L. rhamnosus* GG (10^8 CFU/ml), or pretreated with *L. rhamnosus* GG for 3 h prior to pathogenic infection. Two complementary assays were used to measure the epithelial barrier function.

First, TER was employed as a marker of intercellular tight junction integrity, because it provides an electrical measurement of barrier function toward passive ion flow and the measurements are inversely related to the permeability of a polarized epithelium to macromolecules, such as mannitol and ^{51}Cr-labeled EDTA (3). TER was measured after 18 h of incubation in the presence of 5% CO_2 at 37°C with a Millicell probe (Millipore Corporation, Bedford, MA), and changes were expressed as percentages of untreated control measurements.

Second, the movement of macromolecules across polarized epithelial cell monolayers was assayed using a macromolecular conjugate probe, Alexa Fluor 647 dextran (10 kDa; Molecular Probes, Eugene, OR) (1). Briefly, 0.2 ml of conjugated dextran suspended in DMEM (Invitrogen) was added to the apical compartment of Transwells, and 0.4 ml of DMEM alone added to the basolateral compartment. After incubation for 5 h at 37°C, samples (0.5 ml) from the basolateral compartment were placed into a 96-well plate (Corning) and analyzed to determine their fluorescent intensity using the Odyssey infrared imaging system (LI-COR Biosciences, Lincoln, NE) at a wavelength of 700 nm. Integrated intensities were expressed relative to the integrated intensity of medium samples from untreated controls.

Analysis of ZO-1 and claudin-1 distribution by confocal microscopy. MDCK-I cells were seeded into 6.5-mm Transwells and infected under the experimental conditions used for TER experiments, as described above. The immunofluores-

cence staining protocol was adapted from the protocol of Zareie et al. (47). Briefly, MDCK-I cell monolayers were rinsed in PBS, and this was followed by fixation and permeabilization in 100% methanol (−20°C) (Caledon Laboratories) for 10 min. Cells were incubated in 5% (vol/vol) normal goat serum (Jackson Immunoresearch, West Grove, PA) in PBS for 1 h at room temperature and then incubated with primary rabbit anti-ZO-1 or rabbit anti-claudin-1 (Zymed, San Francisco, CA) for 1 h at 37°C. After unbound primary antibodies were rinsed away with PBS, cells were incubated with secondary Cy2-conjugated goat anti-rabbit IgG (1:200 dilution; Zymed) for 1 h at room temperature. Host cell nuclei were then counterstained with 300 nM 4′,6-diamidino-2-phenylindole dilactate (DAPI) (Molecular Probes) in PBS for 5 min. Monolayers were thoroughly rinsed with PBS, excised from the wells, mounted on slides, and examined with a confocal laser scanning microscope at 1-μm intervals (Zeiss LSM510; Zeiss, Frankfurt, Germany).

Western blotting for tight junction proteins. (i) Protein extraction. Western blotting for tight junction proteins was performed as previously described (47) using MDCK-I whole-cell protein extracts. In addition, MDCK-I cells grown on 6.5-mm Transwells were processed for protein extraction using a Triton X-100-containing lysis buffer, as previously described (26), to separate detergent-soluble protein fractions from detergent-insoluble (cytoskeletal) protein fractions. The initial studies were performed with 12-mm Transwells to increase the protein yield. There were substantial functional differences between cells grown on 6.5-mm Transwells and cells grown on 12-mm Transwells; therefore, subsequent experiments were carried out using 6.5-mm Transwells. To ensure equal protein loading for electrophoresis, protein concentrations were determined using the standard Bradford assay (Bio-Rad Laboratories, Hercules, CA).

(ii) Electrophoresis and immunoblotting. As described by Zareie et al. (47), samples were run on a 12% polyacrylamide Tris-HCl gel (Ready Gel; Bio-Rad Laboratories, Hercules, CA) at 175 V for 45 min (for claudin-1) or on a 7.5% polyacrylamide gel at 111 V for 80 min (for ZO-1), transferred onto a nitrocellulose membrane (BioTrace NT; Pall Corporation, Ann Arbor, MI), blocked for 1 h with Odyssey blocking buffer (LI-COR Biosciences), and probed overnight with either rabbit anti-claudin-1 (1:1,000) or rabbit anti-ZO-1 (1:2,500) together with mouse anti-β-actin (1:5,000; Sigma, St. Louis, MO). Membranes were then probed with IRDye 800 goat anti-rabbit IgG (1:10,000; Rockland Immunochemicals, Gilbertsville, PA) and Alexa Fluor 680 goat anti-mouse IgG (1:20,000; Molecular Probes). Blots were imaged using an infrared imaging system (Odyssey) using both 700- and 800-nm channels at 169-μm resolution. Quantification was performed with commercial analysis software provided by LI-COR. Western blot intensity measurements for whole-cell proteins were determined from the ratio of the integrated intensity of the claudin-1 or ZO-1 band to the integrated intensity of the β-actin band in the same sample. The resulting ratios were normalized using untreated samples included in each experiment and were expressed as percentages (47). For Triton X-100 fractionation extraction, a ratio of the integrated intensity of the claudin-1 band in the soluble fraction to the total claudin-1 band intensity (sum of the signals from soluble and insoluble fractions) was calculated.

Statistics. The results were expressed as means ± standard errors of the means. Statistical differences between multiple groups were calculated using analysis of variance (ANOVA). To examine differences between two experimental groups, the unpaired Student *t* test was employed. A P value of <0.05 was considered statistically significant.

RESULTS

Coincubation of *E. coli* O157:H7 with viable *L. rhamnosus* GG or culture supernatants does not affect the growth of the pathogen. There was no difference in growth when *E. coli* O157:H7 was grown alone in Penassay broth (147 ± 91.1 CFU) and when the pathogen was coincubated with the probiotic (183.6 ± 156.2 CFU) ($P = 0.85$) for 18 h (comparable results were obtained with a coincubation time of 3 h [data not shown]). Similarly, incubation of *E. coli* O157:H7 in *L. rhamnosus* GG culture supernatant did not affect the growth of the pathogen (97.5 ± 92.5 CFU, compared to 66.0 ± 32 CFU for *E. coli* O157:H7 grown in PBS alone [$P = 0.78$]).

***L. rhamnosus* GG pretreatment prevents *E. coli* O157:H7-induced ultrastructural changes in polarized epithelial monolayers.** Transmission electron microscopy of untreated MDCK-I epithelial cells revealed normal cell morphology architecture with intact microvilli and nuclei. In addition, electron-dense tight junctions demonstrated that there were intact intercellular membrane appositions (Fig. 1a). Comparable ultrastructural architecture was seen in epithelial cell monolayers treated with *L. rhamnosus* GG alone (Fig. 1b). In contrast, epithelial cells infected with *E. coli* O157:H7 (Fig. 1c) had intracellular vacuoles, and there were distinct gaps in the continuity of intercellular membrane contacts. Probiotic pretreatment prior to EHEC infection (Fig. 1d) preserved the intercellular contacts but did not prevent cytoplasmic vacuolization.

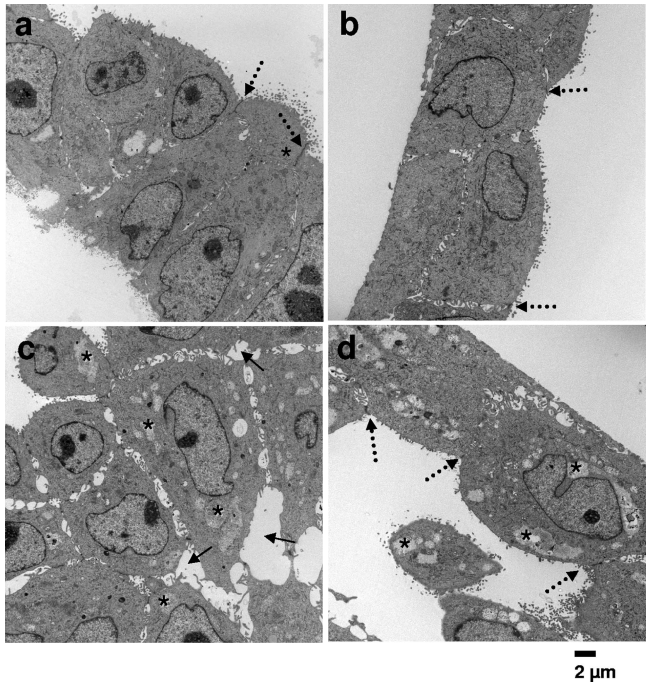

FIG. 1. *L. rhamnosus* GG inhibits *E. coli* O157:H7-induced ultrastructural changes of host cells. (a) Transmission electron photomicrograph of untreated MDCK-I cells showing intact microvilli, normal cellular morphology, and tight junctions (dashed arrows). (b) Probiotic-treated MDCK-I cells with normal cellular morphology. (c) Disruption of MDCK-I cell intercellular tight junctions, increased intercellular spacing (solid arrows), and disturbance in the intracellular compartment (asterisks) with *E. coli* O157:H7 infection. (d) Probiotic pretreatment ameliorates tight junction disruption (dashed arrows) and partially prevents residual morphological changes due to *E. coli* O157:H7 infection (asterisks). Original magnifications, approximately ×5,000.

***L. rhamnosus* GG prevents *E. coli* O157:H7-induced rearrangements of the epithelial cell cytoskeleton.** Phase-contrast and indirect immunofluorescence imaging of MDCK-I and T84 cells infected for 3 h with *E. coli* O157:H7 (10^7 CFU/ml) revealed pathogen binding (Fig. 2a) and bacterium-induced A/E lesions, as indicated by the formation of α-actinin foci (Fig. 2b). Adhesion of *L. rhamnosus* GG (10^8 CFU/ml) to MDCK-I cells did not result in the formation of α-actinin foci (data not shown). Preincubation of the epithelial cells for 1 h at 37°C with *L. rhamnosus* GG prior to *E. coli* O157:H7 infection inhibited pathogen attachment (Fig. 2c) and attenuated bacterium-induced A/E lesion formation (Fig. 2d). By contrast, preincubation of epithelial cells with heat-killed *L. rhamnosus*

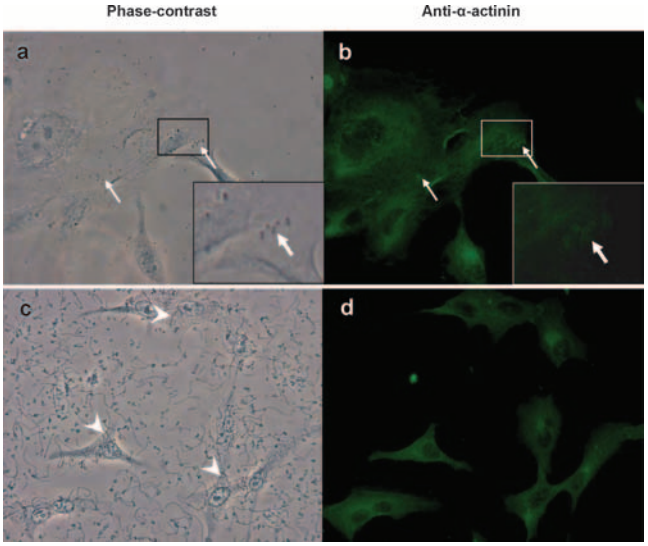

FIG. 2. *L. rhamnosus* GG inhibits *E. coli* O157:H7-induced rearrangements of α-actinin in MDCK-I and T84 epithelial cells. (a) Phase-contrast photomicrographs showing binding of *E. coli* O157:H7 (arrows) to epithelial cells following infection for 3 h at 37°C. (b) Fluorescence photomicrographs showing the aggregation of α-actinin under adherent *E. coli* O157:H7 (arrows). (c) Adherence of *L. rhamnosus* GG bacteria to MDCK-I cells (arrowheads) in the presence of *E. coli* O157:H7 infection. (d) *L. rhamnosus* GG pretreatment reduces α-actinin reorganization in MDCK-I cells infected with *E. coli* O157:H7. Original magnifications, approximately ×400 (inserts, ×1,000). Similar results were obtained for T84 epithelial cells (data not shown).

GG prior to EHEC infection did not prevent pathogen attachment and A/E lesion formation (data not shown).

Semiquantitative analysis of the number of A/E foci in MDCK-I cells pretreated with probiotics prior to *E. coli* O157:H7 showed that there was a decrease in A/E lesions (1.8 ± 1.1 foci/cell) compared with cells infected with the pathogen alone (7.5 ± 1.9 foci/cell) ($P = 0.01$). Probiotic-pretreated T84 cells also had decreased numbers of *E. coli* O157:H7-induced A/E lesions (2.6 ± 0.8 foci/cell with EHEC infection alone and 0.2 ± 0.6 foci/cell with *L. rhamnosus* GG pretreatment and EHEC infection; $P = 0.04$). By contrast, there was no decrease in the number of foci of α-actinin when heat-killed *L. rhamnosus* GG was added to MDCK-I or T84 cell monolayers for 1 h at 37°C prior to challenge with the bacterial pathogen (for MDCK-I, 6.6 ± 2.3 foci/cell; and for T84, 7.4 ± 3.0 foci/cell).

***L. rhamnosus* GG attenuates *E. coli* O157:H7-induced decreases in TER.** Two complementary polarized epithelial cell lines (MDCK-I and T84) were used to assess barrier function in response to EHEC infection in the absence or presence of probiotics. Treatment of polarized epithelial cells with *L. rhamnosus* GG alone did not alter the TER of polarized T84 cell monolayers (which was 92.1% ± 5.9% of the TER of uninfected control monolayers; $n = 12$) (Fig. 3a) and MDCK-I cell monolayers (95.5% ± 4.5%; $n = 5$) (Fig. 3b). Similarly, heat-killed probiotic *L. rhamnosus* GG did not alter the TER of T84 cell monolayers (96.8% ± 0.8%; $n = 5$) or MDCK-I cell monolayers (100%; $n = 3$). As observed previously (47), *E. coli* O157:H7 infection resulted in reduced TER of both T84 cells (19.0% ± 3.0%; $n = 12$) and MDCK-I cells (27.9% ± 11.0%; $n = 5$) cells. Pretreatment of polarized monolayers with *L.*

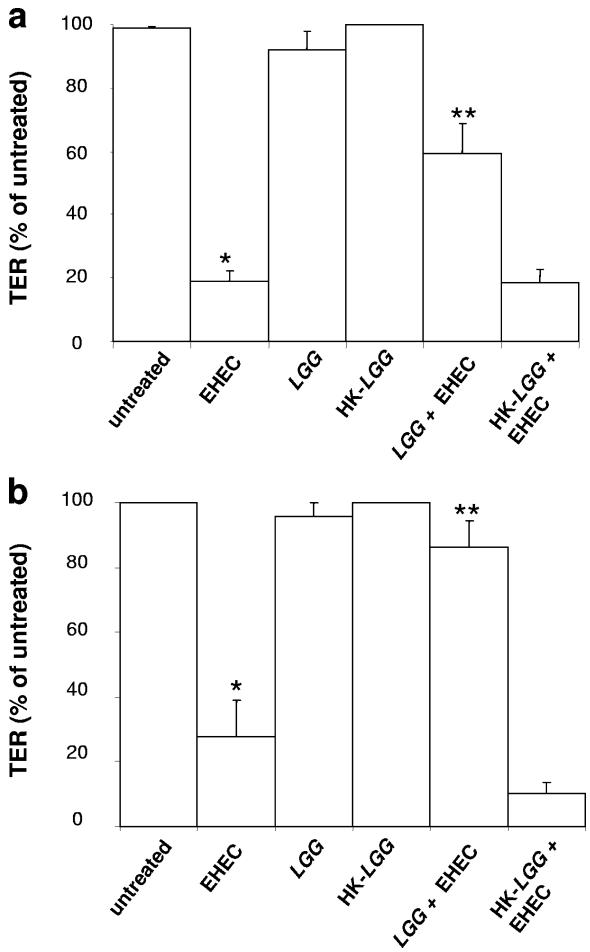

FIG. 3. *L. rhamnosus* GG attenuates *E. coli* O157:H7-induced decreases in TER in T84 and MDCK-I cells. Pretreatment of polarized T84 (a) and MDCK-I (b) monolayers with *L. rhamnosus* GG (10^8 CFU in 0.2 ml) for 3 h prior to infection with *E. coli* O157:H7 (10^7 CFU in 0.2 ml, for 16 to 18 h) decreases the pathogen-induced decrease in TER. One asterisk, $P < 0.05$ for a comparison to untreated cells, as determined by ANOVA; two asterisks, $P < 0.01$ for a comparison to *E. coli* O157:H7-infected cells, as determined by ANOVA. *LGG*, *L. rhamnosus* GG; HK-*LGG*, heat-killed *L. rhamnosus* GG.

rhamnosus GG for 3 h prior to infection attenuated the EHEC-induced decrease in TER (T84 cells, 59.21% ± 9.6% [$n = 12$]; MDCK-I cells, 86.3% ± 8.1% [$n = 5$]). By contrast, amelioration of the reduced TER in response to EHEC infection was not observed when T84 epithelial cell monolayers (18.37% ± 4.4% of the control value; $n = 5$) and MDCK-I epithelial cell monolayers (10.5% ± 3.3%; $n = 3$) were pretreated with heat-killed *L. rhamnosus* GG.

Increases in macromolecular permeability of T84 and MDCK-I cells in response to EHEC infection are attenuated by pretreatment with *L. rhamnosus* GG. Macromolecular permeability assays with T84 cell monolayers using an infrared-sensitive dextran (10-kDa) probe (Fig. 4a) demonstrated that *L. rhamnosus* GG treatment alone did not increase the diffusion of the probe (as measured by the signal intensity for basal medium samples) from apical to basolateral Transwell compartments (relative integrated intensity [RI] compared to untreated monolayers, 1.4 ± 0.4; $P > 0.05$; $n = 4$). In addition, *E.*

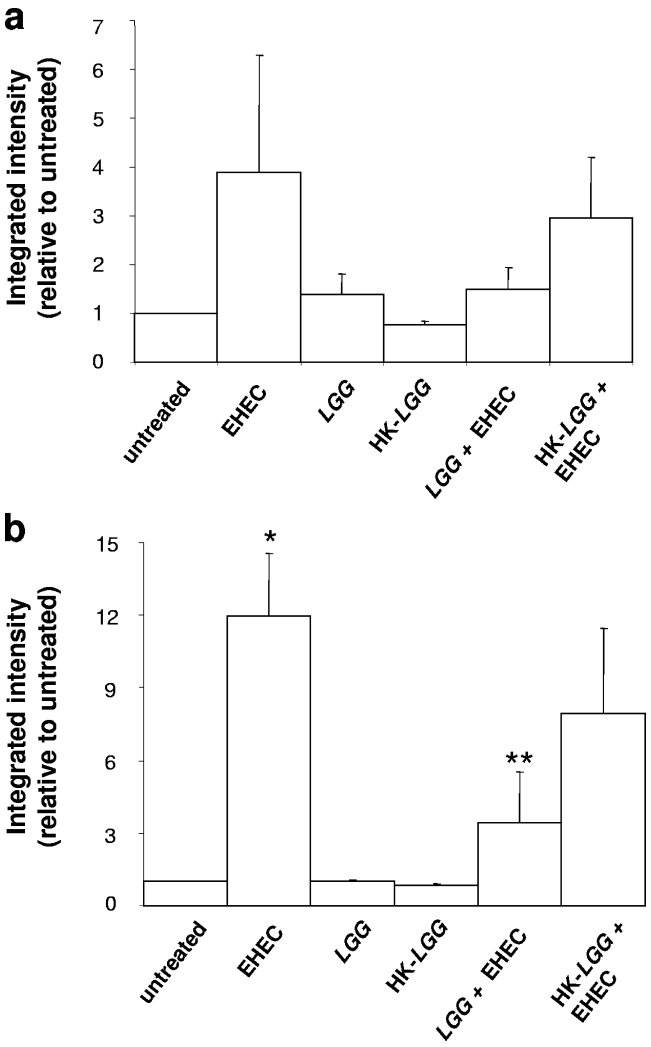

FIG. 4. *L. rhamnosus* GG decreases EHEC-induced increases in macromolecular permeability. Integrated intensities of dextran diffused into the basolateral compartments of Transwells containing T84 cells (a) and MDCK-I cells (b) 5 h after addition to the apical compartment. Polarized monolayers were pretreated with *L. rhamnosus* GG for 3 h prior to infection with *E. coli* O157:H7. One asterisk, $P < 0.05$ for a comparison to untreated cells, as determined by ANOVA; two asterisks, $P < 0.01$ for a comparison to *E. coli* O157:H7-infected cells, as determined by ANOVA. The data represent results from four independent experiments for T84 cells and from three independent experiments for MDCK-I cells. *LGG*, *L. rhamnosus* GG; HK-*LGG*, heat-killed *L. rhamnosus* GG.

coli O157:H7-infected monolayers did not exhibit a marked increase in the permeability to the dextran probe (RI, 3.9 ± 2.4; $P > 0.05$; $n = 4$). Likewise, pretreatment of T84 cell monolayers with viable probiotic for 3 h prior to pathogen infection did not affect the permeability compared to that of untreated cells (RI, 1.5 ± 0.4; $P > 0.05$; $n = 4$), nor did pretreatment of T84 cell monolayers with heat-killed probiotic (RI = 2.96 ± 1.2, $P > 0.05$; $n = 4$).

Pathogen-induced increases in the dextran permeability of MDCK-I cell monolayers (RI compared to uninfected controls, 11.9 ± 2.6; $P < 0.01$; $n = 3$) (Fig. 4b) were reduced when epithelial cells were also pretreated with *L. rhamnosus* GG (RI, 3.42 ± 2.1, $P < 0.05$; $n = 3$). Attenuation of increased macromolecular permeability was not observed when monolayers were pretreated with heat-killed *L. rhamnosus* GG (RI, 7.35 ± 3.5, $P > 0.05$; $n = 3$). Treatment of MDCK-I cell monolayers with viable *L. rhamnosus* GG alone did not affect the dextran permeability compared to that of untreated cells (RI, 1.0 ± 0.1; $P > 0.05$; $n = 3$), nor did treatment with heat-killed *L. rhamnosus* GG alone (RI, 0.9 ± 0.03; $P > 0.05$; $n = 3$).

***L. rhamnosus* GG prevents pathogen-induced redistribution or expression of ZO-1 and claudin-1.** Untreated MDCK-I cells and monolayers treated with *L. rhamnosus* GG alone had intact tight junctions, as demonstrated by continuous and circumferential ZO-1 distribution visualized by confocal immunofluorescence microscopy (Fig. 5a and c, respectively). In contrast, fragmented ZO-1 staining was observed in cells infected with *E. coli* O157:H7 alone (Fig. 5b). Pretreatment with *L. rhamnosus* GG for 3 h prior to EHEC infection prevented these changes (Fig. 5d).

Corresponding *z*-line stacks (*xz* plane) of the en face images (Fig. 5e) demonstrated that there was apically polarized distribution of ZO-1 in untreated cells and monolayers treated with *L. rhamnosus* GG alone. In contrast, punctuate ZO-1 staining was scattered throughout the depth of the cell monolayers infected with O157:H7 alone, indicating a loss of polarization (29). Pretreatment of MDCK-I cells with *L. rhamnosus* GG prior to EHEC infection resulted in prevention of EHEC-induced disruption of epithelial cell polarization.

Western blotting of epithelial whole-cell protein extracts (Fig. 5f) showed that there was a reduction in ZO-1 expression (doublet seen in the 220-kDa region of control samples) in *E. coli* O157:H7-infected cells (band intensity, 0.65 ± 0.13; $P < 0.05$, as determined by ANOVA,; $n = 4$) compared to the expression in untreated monolayers (band intensity, 1). Treatment of MDCK-I cells with probiotics alone maintained the intensity at levels similar to that of the control (band intensity, 0.85 ± 0.14). Epithelial cell monolayers treated with probiotics prior to *E. coli* O157:H7 infection maintained higher levels of ZO-1 expression than monolayers infected with the pathogen alone (band intensity, 0.86 ± 0.09; $P < 0.05$, as determined by ANOVA; $n = 4$). Western blots of Triton X-100-soluble and Triton X-100-insoluble fractionated protein extracts from untreated, EHEC O157:H7-infected, *L. rhamnosus* GG-treated, and *L. rhamnosus* GG-pretreated EHEC O157:H7-infected cells demonstrated that ZO-1 was found only in the Triton X-100-insoluble fractions and not in the soluble fractions ($n = 4$) (Fig. 5g).

The claudin-1 distribution in untreated MDCK-I cells (Fig. 6a) and probiotic-treated cells (Fig. 6c) showed that there was continuous protein distribution circumscribing the epithelial cells, compared to the more diffuse and fragmented pattern of staining in cells infected with EHEC O157:H7 (Fig. 6b). Pretreatment of MDCK-I cells with *L. rhamnosus* GG prior to pathogen infection prevented the changes in claudin-1 redistribution caused by *E. coli* O157:H7 (Fig. 6d). Claudin-1 polarization was disrupted when eukaryotic cells were infected with *E. coli* O157:H7 alone, but these effects were ameliorated by *L. rhamnosus* GG pretreatment (Fig. 6e). As shown in Fig. 6f, Western blotting to determine levels of whole-cell claudin-1 expression demonstrated that there was no change in mono-

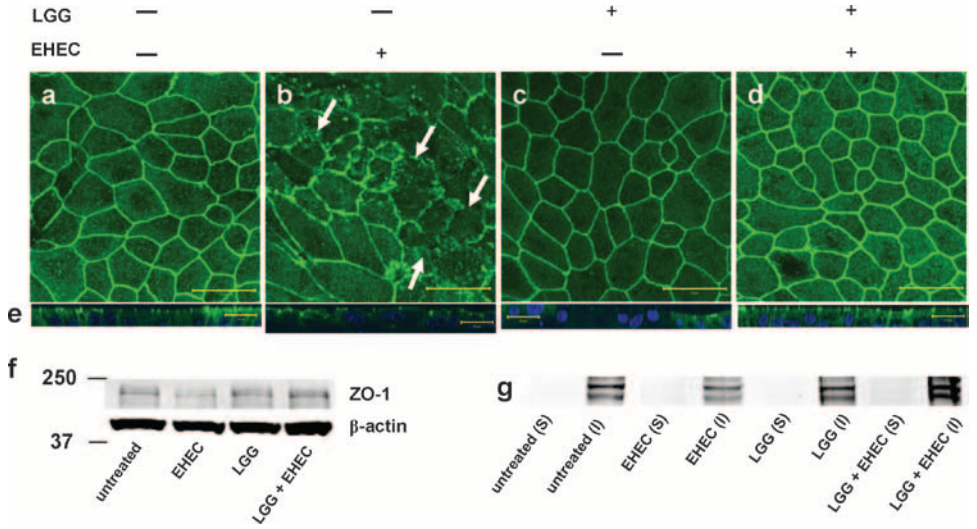

FIG. 5. *L. rhamnosus* GG prevents ZO-1 redistribution and decreased protein expression in *E. coli* O157:H7-infected polarized monolayers. (a) Polarized untreated MDCK-I cell monolayer labeled with rabbit anti-ZO-1 (green), showing continuous, intact circumferential (intercellular) tight junction distribution. (b) *E. coli* O157:H7-infected cells with disturbed ZO-1 band morphology indicated by strand breakage and diffuse staining patterns (arrows). (c) Probiotic-treated cells with intact tight junction distribution. (d) Pretreatment with probiotic 3 h prior to *E. coli* O157:H7 infection, showing intact circumferential tight junctions. (e) *xz* plane images of the corresponding en face micrographs showing epithelial polarization. Nuclei were stained with DAPI (blue). (f) Representative Western blot for ZO-1 in MDCK-I whole-cell protein extracts. β-Actin bands were used as an indicator of protein loading. *L. rhamnosus* GG pretreatment reduced decreased ZO-1 protein expression due to *E. coli* O157:H7 infection. (g) Representative Western blot for ZO-1 in Triton X-100-soluble (S) and Triton X-100-insoluble (I) protein fractions. The confocal micrographs are representative of at least three independent experiments. En face images were captured using an optical magnification of ×630 and were digitally magnified (using the microscope scanning control software) by 2. Scale bars = 20 μm. The Western blots are representative of four independent experiments. LGG, *L. rhamnosus* GG.

layers under any of the experimental conditions (control band intensity, 1.00; band intensity with *E. coli* O157:H7 alone, 0.78 ± 0.01; band intensity with *L. rhamnosus* alone, 0.70 ± 0.03; band intensity for cells pretreated with probiotic prior to pathogen infection, 0.72 ± 0.03; $P = 0.10$, as determined by ANOVA; $n = 4$). Similarly, Western blots (Fig. 6g) of Triton X-100-soluble and Triton X-100-insoluble protein extracts from *E. coli* O157:H7-infected MDCK-I cells did not show that there was a sta-

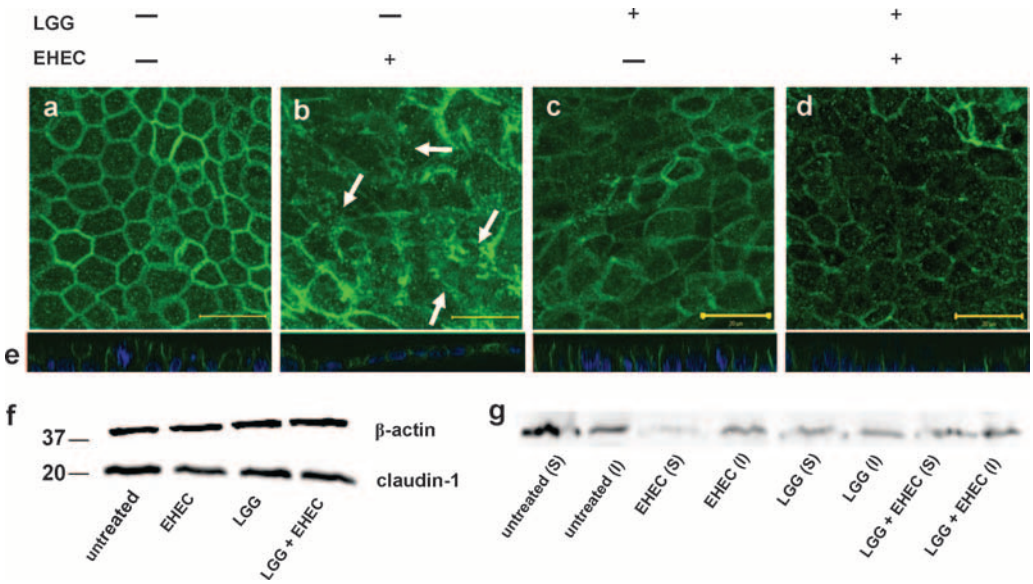

FIG. 6. *L. rhamnosus* GG prevents claudin-1 redistribution in EHEC-infected epithelial monolayers. (a) Untreated MDCK-I cell monolayer labeled with rabbit anti-claudin-1 (green), showing intact intercellular tight junction distribution. (b) *E. coli* O157:H7-infected cells with diffuse claudin-1 staining (arrows). (c) Probiotic-treated cells with normal distribution of claudin-1. (d) Cells pretreated with probiotic 3 h prior to *E. coli* O157:H7 infection, showing normal claudin-1 staining. (e) *xz* plane images of the en face micrographs depicting epithelial polarization. Nuclei were stained with DAPI (blue). (f) Representative Western blot for claudin-1 in MDCK-I whole-cell protein extracts. β-Actin bands were used as an indicator of protein loading. (g) Representative Western blot for claudin-1 in Triton X-100-soluble (S) and Triton X-100-insoluble (I) protein fractions. The confocal micrographs are representative of at least three independent experiments. En face images were captured using an optical magnification of ×630 and were digitally magnified (using the microscope scanning control software) by 2. Scale bars = 20 μm. The Western blots are representative of at least three independent experiments. LGG, *L. rhamnosus* GG.

tistically significant shift in the distribution of claudin-1 from the soluble fraction to the insoluble fraction compared to untreated cells, monolayers treated with probiotics alone, or cells pretreated with probiotics prior to *E. coli* O157:H7 infection (the ratios of the soluble fraction band intensity to the sum of the band intensities for both the soluble and insoluble fractions were 0.78 ± 0.05 for uninfected cells, 0.55 ± 0.06 for EHEC-infected cells, 0.70 ± 0.05 for *L. rhamnosus* GG-treated cells, and 0.66 ± 0.06 for *L. rhamnosus* GG-treated cells prior to EHEC infection; $P = 0.10$, as determined by ANOVA; $n = 3$).

DISCUSSION

Although many clinical studies have reported that probiotics, such as *L. rhamnosus* GG, have beneficial health effects (11, 13, 27, 33), it is still difficult to ascertain their direct mechanism(s) of action. Therefore, the current trend in research in this field is to determine the mechanisms by which particular strains of probiotic bacteria are efficacious in treating specific gut abnormalities or protect against defined microbial infections (35).

We have previously shown that in vivo use of a probiotic mixture containing *L. rhamnosus* R0011 and *Lactobacillus helveticus* R0052 in mice is beneficial in ameliorating intestinal injury in response to *C. rodentium* (19, 20), gastric injury in response to *Helicobacter pylori* infection (21), and stress-induced barrier dysfunction in epithelial ultrastructure in the colon of stressed rats (48). The response to a nonspecific injury, such as stress, leads to defective mucosal barrier function, enhanced luminal bacterial adherence, and alterations in cellular morphology (40, 41). Other investigators have demonstrated that probiotics, such as *Lactobacillus casei* strain DN-114 001, preserve barrier function in polarized T84 and Caco-2 cells infected with adherent-invasive *E. coli* and enteropathogenic *E. coli* strain E2348/69 (14, 31). Isolauri et al. previously demonstrated that suckling rats treated with *L. casei* GG have fewer gastrointestinal permeability disorders induced by cow's milk (16). Interestingly, Yan et al. (46) demonstrated that secreted proteins of *L. rhamnosus* GG prevent tumor necrosis factor alpha-induced apoptosis in human and mouse epithelial cells. Taken together, these studies support the protective effect that probiotics have on the host against pathogenic bacteria.

Probiotics are reported to exert their beneficial effects by producing bacteriostatic or bactericidal agents (6, 42), competitively excluding pathogenic bacteria (37), or regulating immunomodulatory effects (25, 34). Silva et al. (38) previously described the ability of *L. rhamnosus* GG to exert bactericidal effects against a variety of pathogens, such as *Pseudomonas*, *Salmonella*, *Clostridium*, and *E. coli* B-44. However, in the present study, such effects were not observed when pathogenic *E. coli* O157:H7 was incubated in the presence of either viable probiotic *L. rhamnosus* GG culture supernatants or *L. rhamnosus* GG-conditioned medium. These findings emphasize differences in individual probiotic species and indicate that the beneficial effects of *L. rhamnosus* GG observed in this study were likely not due to a reduction in the absolute number of pathogenic bacteria present.

This study broadens our current understanding of how probiotics exert their beneficial effects and emphasizes the ability of *L. rhamnosus* GG (= ATCC 53101) to protect polarized epithelial cells against the effects of *E. coli* O157:H7-induced changes in barrier function at several different levels. Using high-resistance in vitro models of barrier function, we demonstrated that exposure of polarized epithelial cells to the viable probiotic before infection with *E. coli* O157:H7 attenuated pathogen-induced alterations in epithelial barrier function. Differences in the effectiveness of *L. rhamnosus* GG pretreatment for the two cell lines used could be attributed to differences in cell physiology with respect to the absorptive (MDCK-I) and secretory (T84) phenotypes (5, 12).

Similar to previous studies (45, 47), this study demonstrated that EHEC O157:H7 disrupts epithelial tight junction structure, including ZO-1 and claudin-1 distribution, in both MDCK-I and T84 tissue culture cells, resulting in decreased TER and increased permeability to macromolecules. Infection models used by other investigators demonstrated that both probiotic mixtures (such as VSL#3) and additional single strains (e.g., *E. coli* Nissle 1917 and *L. casei* DN-114 001) prevent ZO-1 redistribution in response to *Salmonella enterica* serovar Dublin and enteropathogenic *E. coli* infections in vitro (30, 31). In our study, *L. rhamnosus* GG pretreatment prior to *E. coli* O157:H7 infection ameliorated the pathogen-induced redistribution of ZO-1. We also demonstrated, for the first time, using immunofluorescence microscopy, that *L. rhamnosus* GG pretreatment stabilizes cellular tight junctions, thereby preventing *E. coli* O157:H7-induced redistribution of the integral tight junction protein claudin-1.

To support microscopy observations, we also employed Western blotting techniques to determine levels of ZO-1 and claudin-1. The infrared-based detection system yielded greater resolution than conventional immunoblotting, and there was a doublet in the 220-kDa range. Previous studies demonstrated that this doublet corresponds to α^+ and α^- isoforms (the amounts of the isoforms may differ in various cell lines) (2). Despite observing a redistribution of ZO-1 by immunofluorescence microscopy, we did not observe a change in the characteristics of detergent solubility (an indicator of protein localization between detergent-insoluble regions of the cell membrane and the rest of the cell [4]) in the control, probiotic-treated, or infected cells. Although this study shows that the immunofluorescence staining pattern of claudin-1 was redistributed in *E. coli* O157:H7-infected epithelia, a statistically significant change in the detergent solubility characteristics of this protein was not observed. Therefore, visible changes in tight junction morphology, as observed by microscopy, does not necessarily indicate a change in detergent solubility characteristics. This conclusion is supported by findings of Boyle et al. (4), who noted that tight junction-associated proteins can be mobilized within a particular fraction rather than between detergent-soluble and -insoluble fractions (4). *E. coli* O157:H7 decreases whole-cell expression of ZO-1 and thereby contributes to decreased barrier function (47). The present study demonstrated that this effect can be ameliorated when *L. rhamnosus* GG is added to a polarized monolayer prior to *E. coli* O157:H7 infection.

Taken together, the results of this study indicate that *L. rhamnosus* GG has the ability to protect against *E. coli* O157:H7-induced damage of the epithelial monolayer barrier function by preventing changes in host cell morphology, A/E lesion

formation, monolayer resistance, and macromolecular permeability. In addition, *L. rhamnosus* GG pretreatment prevents *E. coli* O157:H7-induced morphological redistribution of intercellular tight junction proteins and a decrease in the expression of ZO-1.

We expanded findings of previous investigators by demonstrating that *L. rhamnosus* GG pretreatment interrupts the infectious processes of *E. coli* O157:H7, without bactericidal activity. By demonstrating the mode of action of this probiotic strain in attenuating *E. coli* O157:H7 infection, we expanded our knowledge regarding the unique protective contributions of this specific probiotic bacterium when it is cultured with epithelial cells. It is increasingly recognized that the effects of probiotics are both species and strain specific (33). Accordingly, it is important to better define how individual probiotics elicit their beneficial effects as biotherapeutic agents against pathogen-induced disorders of the gastrointestinal tract.

ACKNOWLEDGMENTS

We thank Yew Meng Heng (Pathology Department, Hospital for Sick Children, Toronto, Canada) for technical assistance with the electron microscopy.

This study was supported by grants from the Canadian Institutes of Health Research (CIHR) and the Crohn's and Colitis Foundation of Canada (Fay Shapiro Cutler Grant in Aid of Research). P.M.S. is the recipient of a Canada Research Chair in Gastrointestinal Disease. K.A.D. and G.S.-T. are recipients of CIHR Canada Graduate Scholarship Master's Awards. K.A.D. received a Dutkevich Foundation and Laboratory Medicine and Pathobiology travel award.

REFERENCES

1. **Amieva, M., and R. Vogelmann.** 2004. Epithelial cells and pathogens—the Odyssey System brings light into the darkness. Tight junction barrier function in epithelial cells. http://www.licor.com/bio/PDF/EpithelialCells.pdf. Accessed, 24 August 2006.
2. **Balda, M. S., and J. M. Anderson.** 1993. Two classes of tight junctions are revealed by ZO-1 isoforms. Am. J. Physiol. **264:**C918–C24.
3. **Berkes, J., V. K. Viswanathan, S. D. Savkovic, and G. Hecht.** 2003. Intestinal epithelial responses to enteric pathogens: effects on tight junction barrier, ion transport, and inflammation. Gut **52:**439–451.
4. **Boyle, E. C., N. F. Brown, and B. B. Finlay.** 2006. *Salmonella enterica* serovar Typhimurium effectors SopB, SopE, SopE2 and SipA disrupt tight junction structure and function. Cell. Microbiol. **8:**1946–1957.
5. **Bradbury, N. A.** 2000. Protein kinase-A-mediated secretion of mucin from human colonic epithelial cells. J. Cell Physiol. **185:**408–415.
6. **Corr, S. C., Y. Li, C. U. Riedel, P. W. O'Toole, C. Hill, and C. G. M. Gahan.** 2007. Bacteriocin production as a mechanism for the antiinfective activity of *Lactobacillus salivarius* UCC118. Proc. Natl. Acad. Sci. USA **104:**7617–7621.
7. **Doron, S., D. R. Snydman, and S. L. Gorbach.** 2005. *Lactobacillus* GG: bacteriology and clinical applications. Gastroenterol. Clin. N. Am. **34:**483–498.
8. **FAO/WHO.** 2001. Joint FAO/WHO expert consultation on evaluation of health and nutritional properties of probiotics in food including powder milk with live lactic acid bacteria, Cordoba, Argentina, 1 to 4 October 2001. http://www.fao.org/es/esn/food/foodandfood_probio_en.stm.
9. **Finlay, B. B., and M. Caparon.** 2005. Bacterial adherence to cell surfaces and extracellular matrix, p. 105–120. *In* P. Cossart, P. Boquet, S. Normark, and R. Rappuoli (ed.), Cellular microbiology, 2nd ed. ASM Press, Washington, DC.
10. **Gorbach, S. L.** 2000. Probiotics and gastrointestinal health. Am. J. Gastroenterol. **95:**S2–S4.
11. **Gotteland, M., S. Cruchet, and S. Verbeke.** 2001. Effect of *Lactobacillus* ingestion on the gastrointestinal mucosal barrier alterations induced by indomethacin in humans. Aliment. Pharmacol. Ther. **15:**11–17.
12. **Hansson, G. C.** 1988. A blood group B-like pentaglycosylceramide is the major complex glycosphingolipid of the Madin-Darby canine kidney epithelial cell line I (MDCK I). Biochim. Biophys. Acta **967:**87–91.
13. **Huebner, E. S., and C. M. Surawicz.** 2006. Probiotics in the prevention and treatment of gastrointestinal infections. Gastroenterol. Clin. North. Am. **35:**355–365.
14. **Ingrassia, I., A. Leplingard, and A. Darfeuille-Michaud.** 2005. *Lactobacillus casei* DN-114 001 inhibits the ability of adherent-invasive *Escherichia coli* isolated from Crohn's disease patients to adhere to and to invade intestinal epithelial cells. Appl. Environ. Microbiol. **71:**2880–2887.
15. **Ismaili, A., D. J. Philpott, M. T. Dytoc, R. Soni, S. Ratnam, and P. M. Sherman.** 1995. Alpha-actinin accumulation in epithelial cells infected with attaching and effacing gastrointestinal pathogens. J. Infect. Dis. **172:**1393–1396.
16. **Isolauri, E., H. Majamaa, T. Arvola, I. Rantala, E. Virtanen, and H. Arvilommi.** 1993. *Lactobacillus casei* strain GG reverses increased intestinal permeability induced by cow milk in suckling rats. Gastroenterology **105:**1643–1650.
17. **Johnson-Henry, K., J. L. Wallace, N. S. Basappa, R. Soni, G. K. P. Wu, and P. M. Sherman.** 2001. Inhibition of attaching and effacing lesion formation following enteropathogenic *Escherichia coli* and Shiga toxin-producing *E. coli* infection. Infect. Immun. **69:**7152–7158.
18. **Johnson-Henry, K. C., K. E. Hagen, M. Gordonpour, T. A. Tompkins, and P. M. Sherman.** 2007. Surface layer extracts from *Lactobacillus helveticus* protect against the effects of enterohemorrhagic *Escherichia coli* O157:H7 infection. Cell. Microbiol. **9:**356–367.
19. **Johnson-Henry, K. C., J. D. Riff, M. Gordanpour, and P. M. Sherman.** 2005. Probiotics in models of gastrointestinal bacterial infections. Nutrafoods **4:**29–36.
20. **Johnson-Henry, K. C., M. Nadjafi, Y. Avitzur, D. J. Mitchell, B.-Y. Ngan, E. Galindo-Mata, N. L. Jones, and P. M. Sherman.** 2005. Amelioration of the effects of *Citrobacter rodentium* infection in mice by pretreatment with probiotics. J. Infect. Dis. **191:**2106–2117.
21. **Johnson-Henry, K. C., D. J. Mitchell, Y. Avitzur, E. Galindo-Mata, N. L. Jones, and P. M. Sherman.** 2004. Probiotics reduce bacterial colonization and gastric inflammation in *H. pylori*-infected mice. Dig. Dis. Sci. **49:**1095–1102.
22. **Kaper, J. B., J. P. Nataro, and H. L. Mobley.** 2004. Pathogenic *Escherichia coli*. Nat. Rev. Microbiol. **2:**123–140.
23. **Lee, Y.-K., K.-Y. Puong, A. C. Ouwehand, and S. Salminen.** 2003. Displacement of bacterial pathogens from mucus and Caco-2 cell surface by lactobacilli. J. Med. Microbiol. **52:**925–930.
24. **Liévin-Le Moal, V., and A. L. Servin.** 2006. The front line of enteric host defense against unwelcome intrusion of harmful microorganisms: mucins, antimicrobial peptides, and microbiota. Clin. Microbiol. Rev. **19:**315–337.
25. **Madsen, K., A. Cornish, P. Soper, C. McKaigney, H. Jijon, C. Yachimec, J. Doyle, L. Jewell, and C. De Simone.** 2001. Probiotic bacteria enhance murine and human intestinal epithelial barrier function. Gastroenterology **121:**580–591.
26. **Mally, A., M. Decker, M. Bekteshi, and W. Dekant.** 2006. Ochratoxin A alters cell adhesion and gap junction intercellular communication in MDCK cells. Toxicology **223:**15–25.
27. **Mastretta, E., P. Longo, A. Laccisaglia, L. Balbo, R. Russo, A. Mazzaccara, and P. Gianino.** 2002. Effect of *Lactobacillus* GG and breast-feeding in the prevention of rotavirus nosocomial infection. J. Pediatr. Gastroenterol. Nutr. **35:**1046–1049.
28. **McCormick, B. A.** 2003. The use of transepithelial models to examine host-pathogen interactions. Curr. Opin. Microbiol. **6:**77–81.
29. **Muza-Moons, M., E. E. Schneeberger, and G. A. Hecht.** 2004. Enteropathogenic *Escherichia coli* infection leads to appearance of aberrant tight junctions strands in the lateral membrane of intestinal epithelial cells. Cell. Microbiol. **6:**783–793.
30. **Otte, J.-M., and D. K. Podolsky.** 2004. Functional modulation of enterocytes by gram-positive and gram-negative microorganisms. Am. J. Physiol. **286:**G613–G626.
31. **Parassol, N., M. Freitas, K. Thoreux, G. Dalmasso, R. Bourdet-Sicard, and P. Rampal.** 2005. *Lactobacillus casei* DN-114 001 inhibits the increase in paracellular permeability of enteropathogenic *Escherichia coli*-infected T84 cells. Res. Microbiol. **156:**256–262.
32. **Pizarro-Cerdá, J., and P. Cossart.** 2006. Bacterial adhesion and entry into host cells. Cell **124:**715–727.
33. **Reid, G., J. Jass, M. T. Sebulsky, and J. K. McCormick.** 2003. Potential uses of probiotics in clinical practice. Clin. Microbiol. Rev. **16:**658–672.
34. **Resta-Lenert, S., and K. E. Barrett.** 2006. Probiotics and commensals reverse TNF-alpha and IFN-gamma-induced dysfunction in human intestinal epithelial cells. Gastroenterology **130:**731–746.
35. **Santosa, S., E. Farnworth, and P. J. Jones.** 2006. Probiotics and their potential health claims. Nutr. Rev. **64:**265–274.
36. **Servin, A. L.** 2004. Antagonistic activities of lactobacilli and bifidobacteria against microbial pathogens. FEMS Microbiol. Rev. **28:**405–440.
37. **Sherman, P. M., K. C. Johnson-Henry, H. Yeung, P. Ngo, J. Goulet, and T. A. Tompkins.** 2005. Probiotics reduce enterohemorrhagic *Escherichia coli* O157:H7 and enteropathogenic *E. coli* O127:H6-induced changes in polarized T84 epithelial cell monolayers by reducing bacterial adhesion and cytoskeletal rearrangements. Infect. Immun. **73:**5183–5188.
38. **Silva, M., N. V. Jacobus, C. Deneke, and S. L. Gorbach.** 1987. Antimicrobial substance from a human *Lactobacillus* strain. Antimicrob. Agents Chemother. **31:**1231–1233.
39. **Simonovic, I., J. Rosenberg, A. Koutsouris, and G. Hecht.** 2000. Enteropathogenic *Escherichia coli* dephosphorylates and dissociates occludin from intestinal epithelial tight junctions. Cell. Microbiol. **2:**305–315.
40. **Söderholm, J. D., P. C. Yang, P. Ceponis, A. Vohara, R. Riddell, P. M.**

Sherman, and M. H. Perdue. 2002. Chronic stress induces mast cell-dependent bacterial adherence and initiates mucosal inflammation in rat intestine. Gastroenterology **123:**1099–1108.
41. **Söderholm, J. D., and M. H. Perdue.** 2001. Stress and the gastrointestinal tract. II. Stress and intestinal barrier function. Am. J. Physiol. Gastrointest. Liver. Physiol. **280:**G7–G13.
42. **Takahashi, M., H. Taguchi, H. Yamaguchi, T. Osaki, A. Komatsu, and S. Kamiya.** 2004. The effect of probiotic treatment with *Clostridium butyricum* on enterohemorrhagic *Escherichia coli* O157:H7 infection in mice. FEMS Immunol. Med. Microbiol. **41:**219–226.
43. **Tarr, P. I., C. A. Gordon, and W. L. Chandler.** 2005. Shiga-toxin-producing *Escherichia coli* and haemolytic uraemic syndrome. Lancet **365:**1073–1086.
44. **Van Itallie, C. M., and J. M. Anderson.** 2006. Claudins and epithelial paracellular transport. Annu. Rev. Physiol. **68:**403–429.
45. **Viswanathan, V. K., A. Koutsouris, S. Lukic, M. Pilkinton, I. Simonovic, M. Simonovic, and G. Hecht.** 2004. Comparative analysis of EspF from enteropathogenic and enterohemorrhagic *Escherichia coli* in alteration of epithelial barrier function. Infect. Immun. **72:**3218–3227.
46. **Yan, F., H. Cao, T. L. Cover, R. Whitehead, M. K. Washington, and D. B. Polk.** 2007. Soluble proteins produced by probiotic bacteria regulate intestinal epithelial cell survival and growth. Gastroenterology **132:**562–575.
47. **Zareie, M., J. D. Riff, K. Donato, D. M. McKay, M. H. Perdue, J. D. Soderholm, M. Karmali, M. B. Cohen, J. Hawkins, and P. M. Sherman.** 2005. Novel effects of the prototype translocating *Escherichia coli*, strain C25 on intestinal epithelial structure and barrier function. Cell. Microbiol. **7:**1782–1797.
48. **Zareie, M., K. C. Johnson-Henry, J. Jury, P.-C. Yang, B.-Y. Ngan, D. M. McKay, M. H. Perdue, J. D. Soderholm, and P. M. Sherman.** 2006. Probiotics prevent bacterial translocation and improve intestinal barrier function in rats following chronic psychological stress. Gut **55:**1553–1560.

Editor: V. J. DiRita